Adhesive and adhesiveless contact mechanics of elastic layers on slightly wavy rigid substrates

Adhesive and adhesiveless contact mechanics of elastic layers on slightly wavy rigid substrates

N. Menga,[1] L. Afferrante,[1,*] and G. Carbone[1,2]

[1]*Department of Mechanics, Mathematics and Management, Politecnico of Bari, V.le Japigia, 182, 70126, Bari, Italy*

[2]*CNR - Institute for Photonics and Nanotechnologies U.O.S. Bari, Physics Department "M. Merlin", via Amendola 173, I-70126 Bari, Italy*

Abstract

The behavior of an elastic layer in contact with a wavy rigid substrate is analyzed depending on layer thickness, substrate geometry, energy of adhesion, for given value of remote applied load or penetration. Two different slab configurations are considered: (i) a free layer with uniform pressure acting on the upper boundary, and (ii) a confined layer with uniform displacement assigned to the upper boundary. These two different geometries have been considered as exemplar cases which are of great relevance in a large number of applications of crucial importance as structural adhesives, pressure sensitive adhesives, coatings and protective adhesives.

Our study shows that the layer thickness affects the contact behavior differently depending on the constraints configuration. In particular, reducing the thickness of the layer makes the latter more or less compliant depending on the considered configuration. Thus, the free layer becomes more sticky and, as the layer thickness is reduced, a increasingly large amount of external work needs to be provided to detach the layer from the substrate. On the contrary, the confined layer significantly stiffens by decreasing the layer thickness. This leads to an increase of the pull-off force for detachment accompanied by a decrease of the energy needed to bring the layer and substrate apart.

Keywords: Contact mechanics, adhesion, pressure sensitive adhesives, coatings.

*Corresponding author. Email:luciano.afferrante@poliba.it,phonenumber:+390805962704

I. INTRODUCTION

Adhesion is of crucial importance in contact mechanics, in biology and in a countless number of engineering and industrial applications, as climbing robots [1–3], adhesive gloves and suits [4], structural adhesives [5, 6], adhesive interlayer in laminated glasses [7, 8], thin coatings in orthopedic implants [9, 10], medical adhesive bands [11], pressure sensitive adhesives [12–14], just to enumerate some of them.

However, adhesion can be deleterious and should be avoided in applications other than the ones just mentioned, as, for example, in microelectromechanical systems (MEMS) [15, 16], where sticking phenomena, attributed to adhesion forces, can cause gluing between a thin micromachined membrane and an adjacent parallel surface [17–19].

In all such applications, the geometrical characteristics and the roughness of the substrate play a major role in controlling the adhesive strength of the joint. In particular, in real systems, roughness can be detrimental to the adhesive strength, because it hinders intimate contact between mating surfaces. Roughness can, in fact, decrease both the pull-off force and the work required to detach the surfaces [20, 21]. However, if the contacting bodies are relatively soft the adhesion may increase in presence of roughness [22–27] and cause the appearance of a very significant hysteresis loop during loading and unloading cycles [28].

Contact and adhesion of rough and textured surfaces is also exploited by natural systems to control, e.g. locomotion, climbing abilities and so forth. To this end it suffices to recall the superior abilities of geckos, lizards, flies, beetles, to move, run and climb all type surfaces however tilted or rough like a cinder block [29–31]. Such natural systems and their adhesion control strategies have indeed inspired researchers to provide opportunities for controlling adhesion in engineered systems [32–38].

The adhesive contact of a semi-infinite body with arbitrary periodic profiles has been studied in Ref [39]. Moreover, an experimental study of adhesion of soft viscoelastic materials on surfaces with periodic roughness is performed in Ref [40], whereas in Ref. [41] the role of adhesion is experimentally analyzed to understand the contact mechanics between model micropatterned surfaces.

In the present paper, we focus on the adhesive contact between finite-sized elastic layers and sinusoidal rigid substrates. In particular, adhesion is made change from zero (adhesive-less case) to high values and two different boundary configurations are considered: a free

layer with uniform pressure acting on the upper boundary (model A), and a confined layer (model B). Our calculations show that the free layer has enhanced adhesive toughness and hence is appropriate in all the applications where 'sticky' adhesion is required. The confined layer, instead, is indicated when large pull-off forces need to be sustained. The simple one length scale profile here considered can be also important to capture the basic features of the mechanism of adhesion on real rough surfaces, which are characterized by roughness on several length scales. In fact, the solution here provided may be used to analyze more general rough substrates, by using a multiscale approach as, for example, suggested in Ref. [42–44].

II. FORMULATION

Figg. 1a and 1b show the adhesive contact between a rigid wavy profile of amplitude Λ and wavelength λ, and an elastic layer of thickness h. We assume that the small-slope approximation holds true, i.e. $\Lambda/\lambda \ll 1$. In the first case (free layer or model A), a uniform pressure p_∞ acts on the upper boundary of the layer. In the second case (confined layer or model B), the layer is confined on the upper boundary by a flat rigid plate, and sticky conditions are assumed to hold at the upper interface.

The reference frame and all quantities needed to completely define the problem are also shown in the figures. In particular, the contact penetration Δ, defined as the distance between the mean plane of the deformed lower profile of the layer and the crests of the sinusoidal indenter, and the mean displacement u_m are related through the total displacement u_T of the rigid substrate by the equation: $u_\mathrm{T} = u_\mathrm{m} + \Delta$. Notice the contact mean separation, defined as $s = \Lambda - \Delta$, vanishes when full contact conditions are established.

Although the confined layer model has been deeply investigated in Ref. [25], in the present work, we recover most of the main results to carry out a comparison with the free layer model and to extend that study to the adhesionless contact case.

The plain strain problem under consideration can be formulated in terms of the elastic displacement field through the Navier equation of elasticity (Ref. [45]). However, different boundary conditions must be considered on the upper edge of the layer depending on the model under investigation. In particular, for the model A, at the upper boundary ($y = h$)

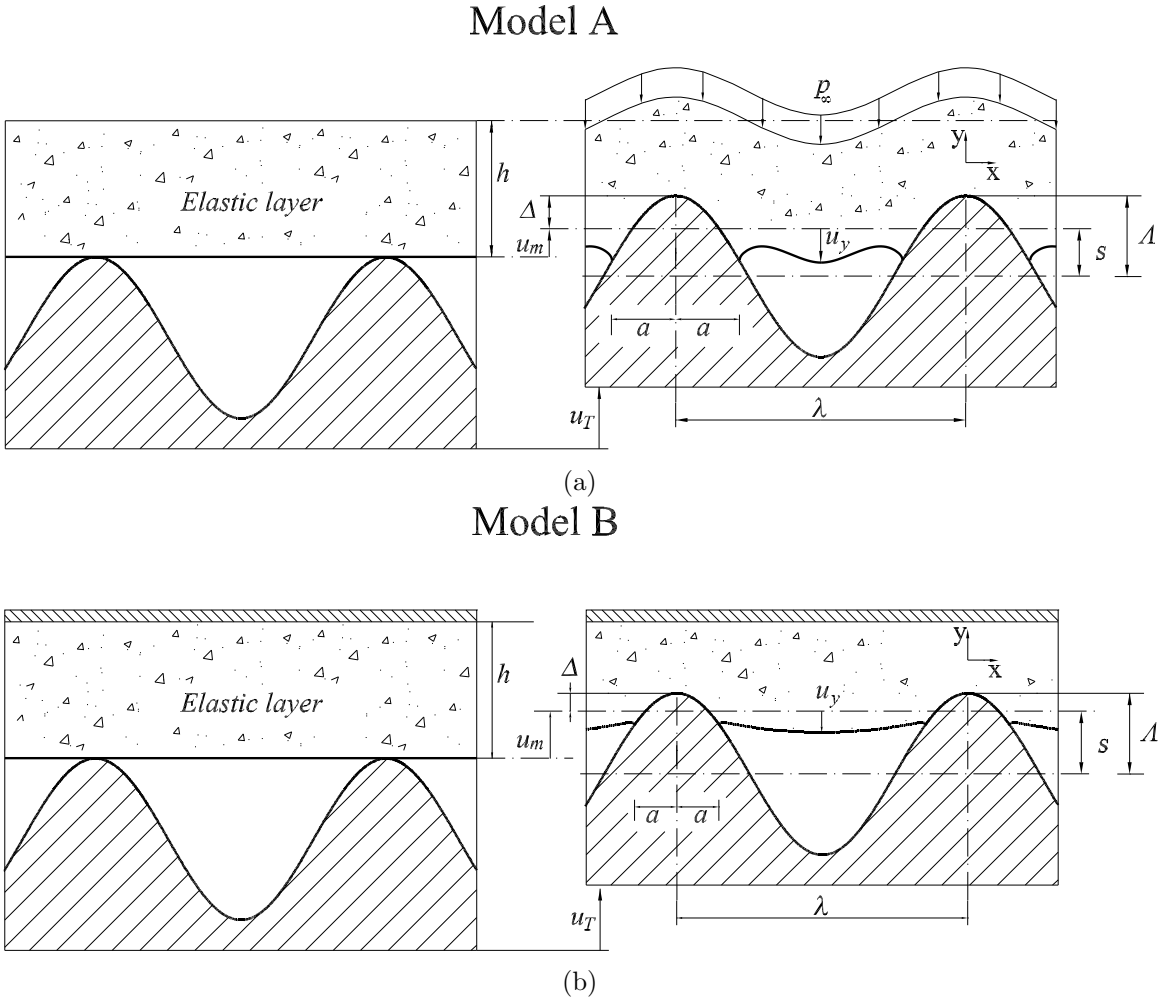

FIG. 1: An elastic layer of thickness h in contact with a rigid slightly wavy profile. Different boundary conditions are considered on the upper layer face: (a) free layer (model A); (b) confined layer (model B).

we have

$$\sigma_{\mathrm{yy}}(x) = p_\infty; \qquad x \in D \tag{1}$$

$$\sigma_{\mathrm{xy}}(x) = 0; \qquad x \in D \tag{2}$$

where $D = [-\lambda/2, \lambda/2]$. For the model B, the above conditions modify in

$$u_{\mathrm{y}}(x) = 0; \qquad x \in D \tag{3}$$

$$u_{\mathrm{x}}(x) = 0; \qquad x \in D \tag{4}$$

At the contact interface ($y = 0$), the boundary conditions in both cases can be written as

$$u_{\mathrm{y}}(x) = r(x) + u_{\mathrm{T}} - \Lambda; \qquad x \in \Omega \tag{5}$$

$$\sigma_{\mathrm{yy}}(x) = 0; \qquad x \in D - \Omega \tag{6}$$

$$\sigma_{\mathrm{xy}}(x) = 0; \qquad x \in D \tag{7}$$

being $\Omega = [-a, a]$ the contact domain, $r(x) = \Lambda \cos(kx)$ the profile of the substrate, and $k = 2\pi/\lambda$.

As shown in Ref. [25], the contact problem can be reduced to a Fredholm equation of the first kind, because of linearity and translational invariance along x. Therefore, the elastic displacement $u_{\mathrm{y}}(x)$ of the layer can be related to the normal contact pressure $p(x)$ through the Green function G calculated at the contact interface. As a result, the original problem reduces to the following Fredholm equation of the first kind

$$-\int_{\Omega} G(x-s)\, p(s)\, ds = \Delta + \Lambda\left[\cos(kx) - 1\right]; \qquad x \in \Omega \tag{8}$$

and, once the contact pressure $p(x)$ is calculated, the normal displacement in the region where the two bodies are not in contact can be evaluated as

$$u_{\mathrm{y}}(x) = u_{\mathrm{m}} - \int_{\Omega} G(x-s)\, p(s)\, ds \qquad x \in D - \Omega \tag{9}$$

In Ref. [46] it has been shown that

$$G(x) = \frac{2(1-\nu^2)}{\pi E}\left(\log\left[2\left|\sin\left(\frac{kx}{2}\right)\right|\right] + \sum_{m=1}^{\infty} A_{\mathrm{m}}(kh)\,\frac{\cos(mkx)}{m}\right) \tag{10}$$

with the only coefficients A_{m} depend on the layer upper boundary conditions, and specifically

$$A_{\mathrm{m}}(kh) = \frac{2mkh + \sinh(2mkh)}{1 + 2(mkh)^2 - \cosh(2mkh)} + 1 \tag{11}$$

for the free layer model (model A) and

$$A_{\mathrm{m}}(kh) = \frac{2hkm - (3-4\nu)\sinh(2hkm)}{5 + 2(hkm)^2 - 4\nu(3-2\nu) + (3-4\nu)\cosh(2hkm)} + 1 \tag{12}$$

for the confined layer model (model B). Moreover, the displacement u_m of the mean plane is given by

$$u_{\mathrm{m}} = \frac{1+\nu}{1-\nu}\frac{1-2\nu}{E}p_{\mathrm{m}}h \tag{13}$$

where $p_{\mathrm{m}} = \lambda^{-1}\int_{\Omega} p\left(x\right)dx$ is the mean contact pressure. Notice p_{m} is just p_{∞} for the free layer model, and u_{m} vanishes for incompressible materials (i.e. when Poisson's ratio $\nu = 0.5$).

A. Method of solution

In order to solve the problem we will follow the procedure described below. For any given value of the penetration Δ, the unknown contact pressure distribution $p\left(x\right)$ can be determined by inverting eq. (8). Once known $p\left(x\right)$, the displacements field can be easily calculated on the whole domain D by eqs. (9, 13). However, to solve eq. (8) we need to know the contact area (i.e. the domain Ω) and, therefore, an additional equation is required. To this end we will distinguish between the adhesive case and the adhesiveless one.

1. Adhesive contact

Under isothermal conditions and for fixed penetration Δ, the contact size a can be calculated by requiring that the total free energy $\mathcal{F}$ is stationary [25]

$$\left(\frac{\partial \mathcal{F}}{\partial a}\right)_{\Delta} = 0 \tag{14}$$

The energy $\mathcal{F}$ is the sum of the interfacial elastic energy $\mathcal{E}$, due to the surface deformation

$$\mathcal{E}\left(a\right) = \frac{1}{2}\int_{D} p\left(x\right)\left[u_y\left(x\right) - u_m\right]dx = \frac{1}{2}\int_{\Omega} p\left(x\right)\left[r\left(x\right) - \Lambda + \Delta\right]dx \tag{15}$$

and the adhesion energy $\mathcal{A}$

$$\mathcal{A}\left(a\right) = -\Delta\gamma\int_{\Omega}\sqrt{1+\left[r'\left(x\right)\right]^2}dx \tag{16}$$

being $\Delta\gamma$ the work of adhesion, also referred as the Duprè energy of adhesion.

Therefore, the set of equations (8, 14) allows to calculate, for given penetration Δ, the contact size a and the contact pressure distribution $p\left(x\right)$.

It is worth noticing that the current formulation involves only the net displacement of the layer, measured with respect to the mean plane of the deformed interface. Results are hence not affected by the mean displacement u_{m} and the approach remains consistent even for $h \to \infty$, when the mean quantities become infinite.

2. Adhesiveless contact

In the absence of adhesion, the condition Eq. (14) simply requires that the energy release rate $\mathcal{G} = -\frac{1}{2}\partial\mathcal{E}/\partial a$ vanishes. In this, case recalling that $\mathcal{G}$ is related to the stress intensity factor $K_I(a) = \lim_{r\to a^-} p(r)\sqrt{2\pi(a-r)}$, through the relation [49]

$$\mathcal{G} = \frac{1-\nu^2}{E} K_I^2 \tag{17}$$

Eq. (14) simply requires that at equilibrium

$$K_I(a) = \lim_{r\to a^-} p(r)\sqrt{2\pi(a-r)} = 0 \tag{18}$$

In the case of adhesiveless contacts Eq. (18) is simpler to use than Eq. (14) as it avoids the numerical instability related to the fact that $\partial\mathcal{G}/\partial a = \partial^2\mathcal{E}/\partial a^2 = 0$ in adhesiveless contacts. Eqs. (8, 18) enable us to solve the contact problem for any given value of the contact penetration Δ.

III. RESULTS AND DISCUSSION

The effects of the layer thickness and substrate geometry on contact properties are investigated and a comparison between model A and B is carried out. Results are given in terms of the following dimensionless quantities $\tilde{h} = kh$, $\tilde{a} = ka$, $\tilde{\Lambda} = k\Lambda$, $\tilde{\Delta} = \Delta/\Lambda$, $\tilde{s} = s/\Lambda$, $\tilde{p} = 2(1-\nu^2)p/(Ek\Lambda)$, $\tilde{\gamma} = (1-\nu^2)k\Delta\gamma/(\pi E)$, $\tilde{\mathcal{F}} = 2(1-\nu^2)\mathcal{F}/(E\Lambda^2)$ and are presented for an incompressible material, i.e. $\nu = 0.5$. Moreover, according to Ref. [25], the adhesive behavior is investigated in terms of the effective energy of adhesion per unit area $\gamma_{\mathrm{eff}} = -\mathcal{F}/\lambda$, a quantity strictly related to the work required to detach the layer from the substrate.

A. Adhesive contact

Let us consider first the case of vanishing mean pressure $p_{\rm m} = 0$, as this condition is of particular interest for coatings adhering on a substrate in absence of external loads. Since equilibrium requires the interfacial free energy $\mathcal{F}$ being stationary, contact occurs when the repulsive effects of the elastic energy due to the surface deformations balance the attractive effects of the adhesion energy.

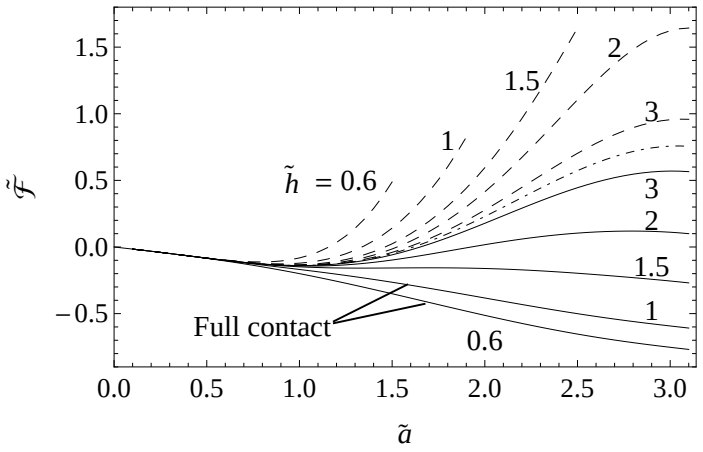

FIG. 2: The dimensionless interfacial free energy $\tilde{\mathcal{F}}$ as a function of the dimensionless contact area $\tilde{a}$ for no-load conditions ($p_m = 0$), $\tilde{\Lambda} = 2$ and $\tilde{\gamma} = 0.05$. Solid lines are relative to the free layer model (model A), dashed lines to the confined layer model (model B). Results are shown for different values of the layer thickness. The halfplane solution is also plotted with dashed-dot line. Notice $\tilde{a} = \pi$ corresponds to full contact.

Fig. 2 shows the dimensionless interfacial free energy $\tilde{\mathcal{F}}$ for both the systems under investigation as a function of the contact area for $\tilde{\gamma} = 0.05$ and $\tilde{\Lambda} = 2$. Solid lines refer to the free layer model (model A), dashed lines to the confined layer model (model B). Results are shown for different values of the layer thickness. Notice the halfplane solution (dashed-dot line) given in Ref. [47] is recovered when $h \to \infty$, independently of the layer configuration.

For the confined layer, partial contact is always stable because it corresponds to the minimum of $\mathcal{F}$. In particular, when $h < \Lambda$, this is the only possible state because complete contact cannot be physically established (the curves are truncated for this reason). When $h > \Lambda$, the system can experience a new state involving complete contact with the substrate, and it will remain in such state even when the external load is removed. This behavior is a consequence of the assumption of the infinitely small range ρ of van der Waals forces, and,

therefore, holds true provided that the local normal pressure at the interface $|p(x)| \leq \sigma_{\text{th}} \approx \gamma/\rho$.

The free layer has a similar behavior when the thickness is sufficiently large (i.e. $\tilde{h} > 1.5$ in the example results given in Fig. 2). In fact, in this case, two partial contact states can occur, but only one corresponds to a stable equilibrium. Further, complete contact is also stable. For thinner layers ($\tilde{h} < 1.5$), only full contact with the rigid substrate can be established. This is easily explained, if one considers that for $h \ll \lambda$ the behavior of the free layer can be modelled by a thin Euler-Bernoulli beam, for which the increase in elastic energy due to pure bending upon the occurrence of full contact can be estimated as $\mathcal{E} = \pi^4 (1-\nu^2)^{-1} E\Lambda^2 (h/\lambda)^3 /3$. The adhesion energy is instead proportional to the real contact length L_{FC} that is larger than λ, because of roughness: $\mathcal{A} = \Delta\gamma L_{FC} = \Delta\gamma [2\lambda \mathrm{E}(-4\pi^2\Lambda^2/\lambda^2)/\pi]$, being $\mathrm{E}(\cdot)$ the complete elliptic integral function. Thus, the condition for the occurrence of full contact is $\mathcal{E} < \mathcal{A}$, which gives

$$\tilde{h} < \tilde{h}_{\text{th}} = \left[96\tilde{\gamma}\mathrm{E}\left(-\tilde{\Lambda}^2\right)/\tilde{\Lambda}^2\right]^{1/3} \tag{19}$$

For $\tilde{\gamma} = 0.05$ and $\tilde{\Lambda} = 2$, we obtain $\tilde{h}_{\text{th}} \approx 1.47$, which is very close to the value calculated in Fig. 2.

Therefore, we can argue that the 'adhesive' effects become dominant under a threshold value of the thickness h_{th}, making the complete contact the only stable state of equilibrium. Interestingly, when Λ vanishes, i.e. the sinusoidal profile is flattened down, h_{th} tends to infinity. Under these conditions, in fact, the substrate is flat and the full contact cannot be avoided anymore.

The above statements find corroboration in Fig. 3, where, for the free layer model, the dimensionless threshold thickness $\tilde{h}_{\text{th}}$, below which the layer snaps into full contact with the substrate, is plotted as a function of the dimensionless amplitude $\tilde{\Lambda}$.

As shown below, the work required to completely detach the layer from the substrate depends on the energy of the current bonded state and on the energy at the moment of pull-off. However, regardless of pull-off occurs under displacement or load controlled conditions, to reduce the work of detachment is certainly useful increasing the energy level of the local minimum of $\mathcal{F}$. In order to achieve this purpose, Fig. 2 shows that we must act differently depending on the layer boundary conditions. In fact, in the case of the model B, we must

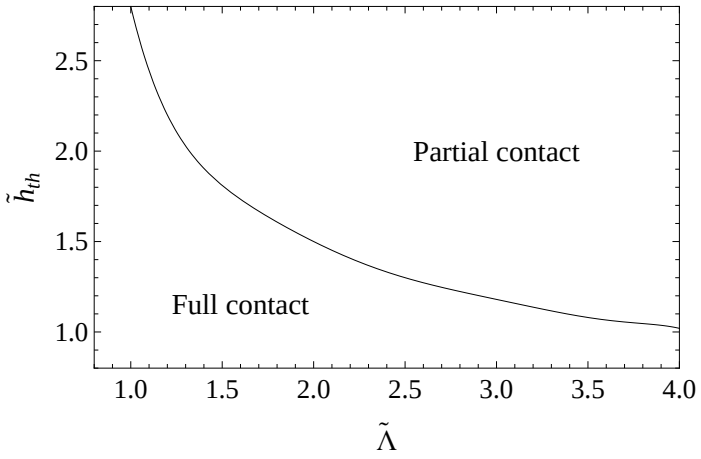

FIG. 3: The variation of the threshold value of the dimensionless thickness $\tilde{h}_{th}$, below which the layer snaps in full contact, with the dimensionless amplitude of the substrate $\tilde{\Lambda}$. Results are relative to the model A and are obtained for no-load conditions ($p_m = 0$) and $\tilde{\gamma} = 0.05$.

reduce the thickness, while the opposite operation is required for the model A.

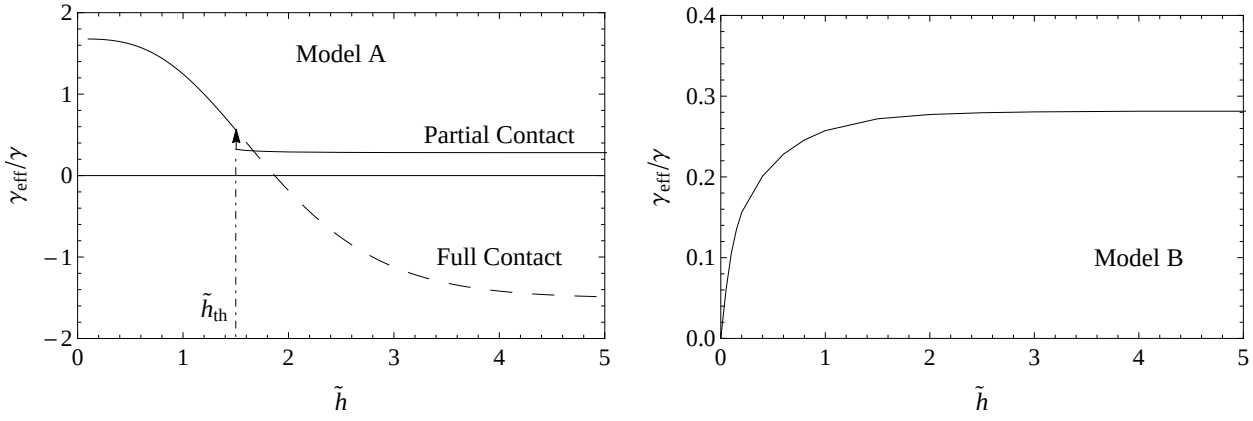

(a) (b)

FIG. 4: The normalized effective energy of adhesion as a function of the dimensionless layer thickness $\tilde{h}$, under no-load conditions ($p_m = 0$). Results are shown both for the model A (a) and the model B (b). Calculations are performed for $\tilde{\Lambda} = 2$ and $\tilde{\gamma} = 0.05$.

Fig. 4 shows the normalized effective energy of adhesion $\gamma_{\rm eff}/\gamma = -\mathcal{F}/(\gamma\lambda)$ as a function of the dimensionless layer thickness, for no-load conditions and $\tilde{\Lambda} = 2$. For the confined layer, (model B), Fig. 4b shows a significant decrease of $\gamma_{\rm eff}/\gamma$ taking place as h is reduced from values less or equal to λ. The reason for such a behavior is provided in Ref. [25], where it is shown that the elastic energy, stored at interface and required to obtain full contact, is $\mathcal{E} \propto (1-\nu^2)^{-1} E\Lambda^2\lambda/h$. As a result, $\mathcal{E}$ significantly increases with decreasing h and, in

turn, the energy of adhesion decreases because higher values of $\mathcal{E}$ lead to a reduction of the effective contact area.

For the free layer case (model A), Fig. 4a shows that when the thickness of the layer is sufficiently high, a stable equilibrium state is established in partial contact conditions (solid line). However, if an external load able to force the system in full contact is added, complete contact would be maintained even removing the load (that is restoring the condition $p_{\mathrm{m}} = 0$).

As the thickness h of the layer is reduced, the elastic strain energy stored at the interface also decreases (being in this case $\mathcal{E} \propto h^3$), thus leading to an increase of the effective energy of adhesion and contact area. When h reaches the threshold value h_{th}, stable equilibrium is possible only under complete contact conditions, and a jump from partial to full contact is observed. We note, that, as the adhesive interactions are modelled as infinite short range forces, this jump is formally irreversible. This means that, starting from this condition, and increasing the thickness even above the threshold value, full contact is maintained and the reduced effective energy of adhesion $\gamma_{\mathrm{eff}}/\gamma$ changes following the dashed line. Of course in a real system the presence of interfacial defects, or even the short length-scale structures of the rough surface, will modify the system behavior and detachment by cracks propagation could occur.

Moreover, for very thin layers, the normalized effective adhesion energy is larger than one. This is easily explained by observing that the elastic energy vanishes as h^3 for $h \to 0$, and by considering that the adhesion energy is proportional to real length of the contact.

Fig. 5 shows the dimensionless contact area (Fig. 5a) and mean separation (Fig. 5b) at the equilibrium as functions of the dimensionless layer thickness $\tilde{h}$, for different values of the dimensionless amplitude $\tilde{\Lambda}$. The results are relative to the free layer model. As expected, moving from partial contact conditions, when the thickness decreases below a threshold value, the elastic layer jumps into full contact with the substrate (see arrows in Fig. 5). It is worth noticing that the contact area (Fig. 5a) reduces as the rigid sinusoidal profile becomes more wavy (i.e. $\tilde{\Lambda}$ increases), whereas the contact mean separation (Fig. 5b) increases. These results are expected because the elastic energy increases with Λ^2, leading to a reduction in the effective energy of adhesion.

Now let us consider the case $p_{\mathrm{m}} \neq 0$ and study the behavior of the two analyzed systems (models A and B) when the controlled parameter is the penetration Δ.

Fig. 6 shows the dimensionless mean pressure as a function of the $\tilde{\Delta}$. Results are given

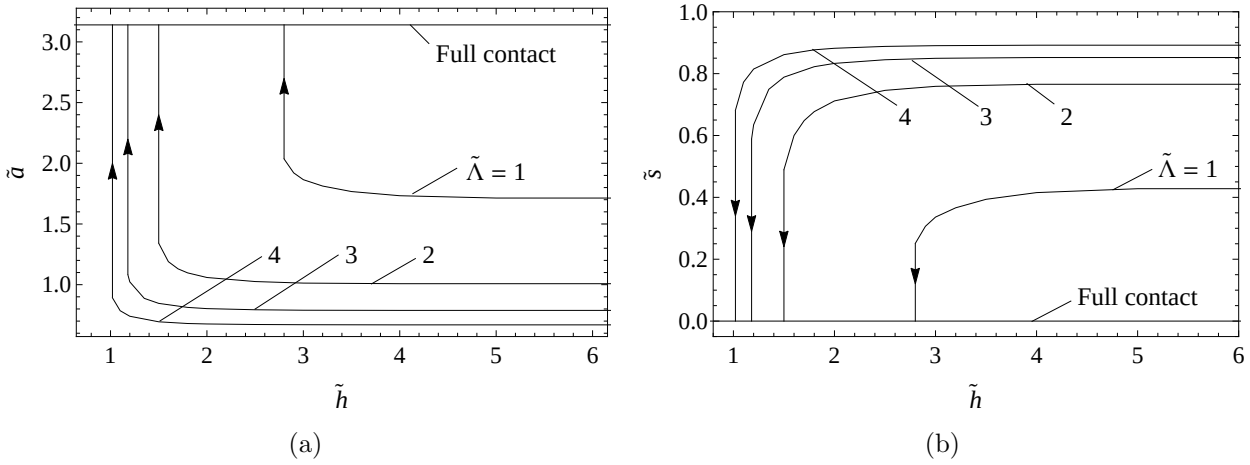

FIG. 5: The dimensionless equilibrium contact size $\tilde{a}$ (a) and dimensionless mean separation $\tilde{s}$ (b) as functions of the dimensionless layer thickness $\tilde{h}$, for the model A. Results are shown for different values of $\tilde{\Lambda}$. Calculations are performed under no-load conditions ($p_m = 0$) and $\tilde{\gamma} = 0.05$. Notice $\tilde{a} = \pi$ and $\tilde{s} = 0$ correspond to full contact.

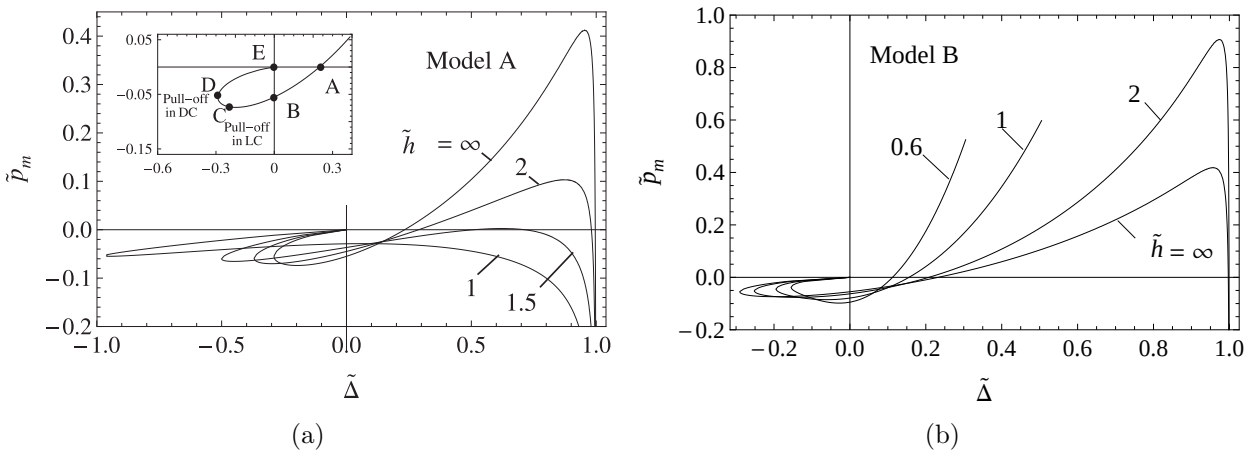

FIG. 6: The mean contact pressure at equilibrium $\tilde{p}_m$ as a function of the dimensionless conact penetration $\tilde{\Delta}$ for different values of the dimensionless layer thickness $\tilde{h}$, $\tilde{\Lambda} = 2$ and $\tilde{\gamma} = 0.05$. Results are shown both for the model A (a) and the model B (b). The inset of 6a shows the pull-off occurence under displacement controlled (point D) or load controlled (point C) conditions. Notice the layer is pushed against the substrate for positive pressures and is pulled away when the pressure becomes negative. The same sign convention is adopted for the displacement.

for $\tilde{\Lambda} = 2$, $\tilde{\gamma} = 0.05$ and different values of $\tilde{h}$. As already observed, the diagrams confirm that the contact stiffness $dp_{\rm m}/d\Delta$ increases or decreases with h depending on the considered layer configuration (model A or model B).

With reference to the model A, at small value of h/λ, the layer behaves as an Euler-

Bernoulli beam, whose stiffness reduces proportionally to h^3. However, for large ratios Λ/h we actually expect the system behaves quite differently. Indeed, under these conditions, the large deformations activate the membrane stress stiffening effects, which are neglected in our formulation. Conversely, in the model B, the layer becomes stiffer as the thickness is reduced because of the presence of the upper rigid constraint which hampers the elastic deformation of the layer. Also in presence of external loads, for the model A, we can define a threshold thickness $h_{\rm th}$, below which partial contact cannot occur. About the model B, complete contact can occur only when the layer thickness is larger than the amplitude Λ of the rigid substrate. In this case, when the mean pressure reaches the maximum peak shown in Fig. 6b, the equilibrium becomes unstable and the layer jumps into full contact.

Moreover, under load controlled conditions, when substrate and layer are approached at zero mean pressure ($p_{\rm m} = 0$), the system jumps into contact and the layer is pulled up to a given displacement (point A in the inset of Fig. 6a). From this point, by applying a squeezing load (positive pressures) the system moves on the right increasing the contact penetration. On the contrary, by applying a tensile load (negative pressures), the system experiences a reduction of the contact penetration. When the penetration vanishes (point B of the inset) the mean plane of the deformed profile becomes tangent to the crests of the sinusoidal substrate. From this point, a further reduction of the mean pressure leads to negative contact penetrations. In this case, the mean plane of the deformed profile lies above the crests of the substrate, but the local displacements (induced by adhesive interactions) still allow the elastic layer to be partially in contact with the substrate. When the pressure corresponding to the point C is reached, the system can no longer sustain a further reduction of the mean pressure, so pull-off occurs. The remaining part of the curve (branch C-E) corresponds to unstable states of equilibrium.

Similar considerations can be drawn when displacement controlled conditions are taken into account. In this case, the stable equilibrium branch extends up to the point D, where pull-off occurs, whereas the branch D-E is the unstable one.

The variation of the dimensionless contact area with the dimensionless mean contact pressure is shown in Fig. 7 for different values of the layer thickness, for $\tilde{\Lambda} = 2$ and $\tilde{\gamma} = 0.05$. For the model A case, under force controlled conditions, unstable equilibrium is obtained on those branches of the curves where an increase of pressure leads to a decrease of the contact area, while stable equilibrium occurs on those branches where the contact area increases

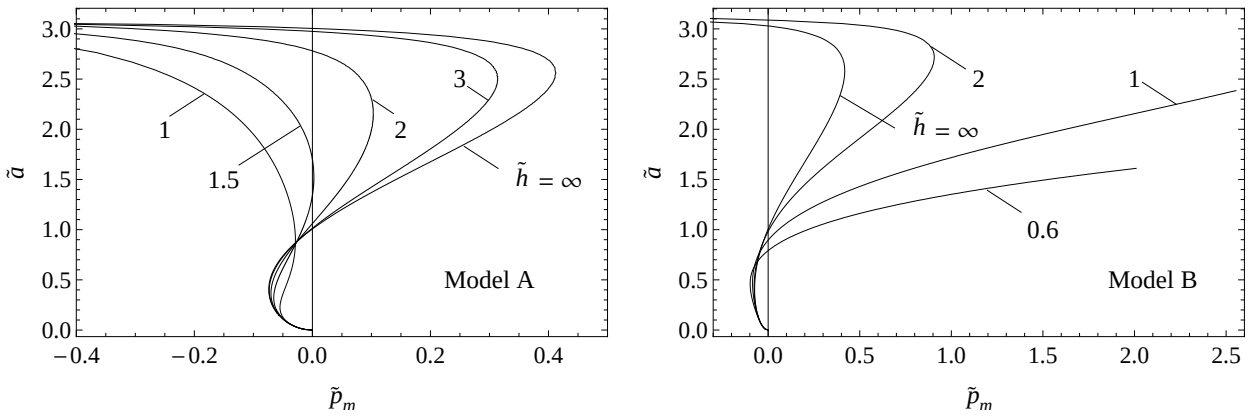

FIG. 7: The dimensionless contact size $\tilde{a}$ at the equilibrium as a function of the dimensionless mean contact pressure $\tilde{p}_m$ for different values of the dimensionless layer thickness $\tilde{h}$, $\tilde{\Lambda} = 2$ and $\tilde{\gamma} = 0.05$. Results are shown both for the model A (a) and the model B (b).

with load. Now let us consider the curves for $\tilde{h} > 1.5$, in this case, as already mentioned, the system lays in partial contact with $p_{\rm m} = 0$. In fact, as soon as the substrate touches the layer, a finite contact area is immediately established due to the action of the adhesive forces, that is to say that the layer jumps into partial contact with the substrate. This process is irreversible, and leads to energy dissipation. The contact area increases with the applied mean pressure until a maximum value of $p_{\rm m}$ is reached which depends, among the other quantities, on the thickness of the layer. Beyond this point, the equilibrium curve (under load controlled conditions) becomes unstable and the systems jumps into full contact with the substrate. Now let us concentrate on the case $\tilde{h} < 1.5$. This time, the entire equilibrium curve is characterized by negative value of the mean pressure $p_{\rm m}$. Thus, as already explained, the layer substrate snaps into full contact with the substrate even at zero applied load.

Moving to the model B case, we observe a similar trend except that when $h < \Lambda$ full contact conditions are geometrically forbidden.

Fig. 8a shows the absolute value of the pull-off pressure as a function of $\tilde{h}$. A different behavior of the two models is again observed: for the model A, $|\tilde{p}_{\rm off}|$ decreases with decreasing the slab thickness, while the opposite behavior occurs for the model B (the latter trend agrees with Ref. [25]).

The variation of the absolute value of the dimensionless critical penetration $\left|\tilde{\Delta}_{\rm off}\right|$, with the dimensionless layer thickness $\tilde{h}$ is shown in Fig. 8b, under displacement controlled

conditions. In such case, with reference to the model A, the critical displacement $\left|\tilde{\Delta}_{\text{off}}\right|$ for detachment increases with decreasing the slab thickness, while the opposite is observed for the model B case.

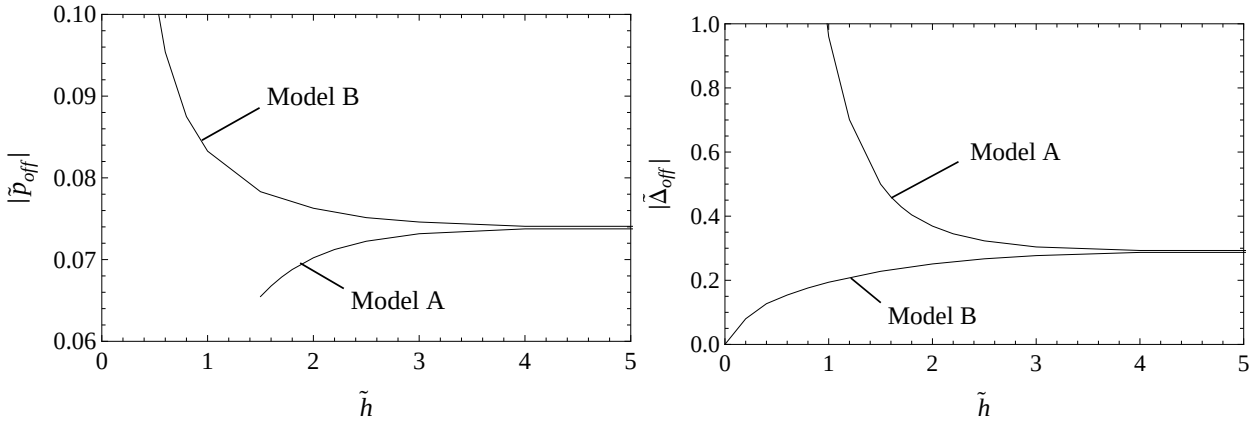

FIG. 8: The dimensionless absolute value of the pull-off contact pressure $|\tilde{p}_{\text{off}}|$ (a) and the dimensionless absolute value of the pull-off displacement $\left|\tilde{\Delta}_{\text{off}}\right|$ (b) as functions of the dimensionless layer thickness. Results given in Fig. 8a are obtained under load controlled conditions, whereas results given in Fig. 8b are obtained in dispacement control. Calculations are perfomed for $\tilde{\Lambda} = 2$ and $\tilde{\gamma} = 0.05$.

The differences observed during the pulling process provide useful suggestions on which type of model (A or B) should be employed depending on the specific application. In this respect, the model B, showing a larger pull-off force, is more suited for structural adhesives, or in general for applications requiring the adhesion to resist to strong impulsive forces. Viceversa, in the model A, the layer is able to face larger deformations, thus showing higher adhesive toughness. To compare the two models from the point of view of their toughness properties it is enough to calculate the work needed to separate the two contacting bodies. In dimensionless terms this work is

$$\tilde{W}_{\text{det}} = 2\pi \int_{\tilde{\Delta}_0}^{\tilde{\Delta}_1} \tilde{p}_{\text{m}} d\tilde{\Delta} \tag{20}$$

where $\tilde{\Delta}_1$ is the dimensionless contact penetration at which pull-off occurs and $\tilde{\Delta}_0$ an arbitrary initial value of the penetration. In particular, we can consider as initial condition the value of $\tilde{\Delta}$ at which the system is in equilibrium in absence of applied external load. Notice the value of $\tilde{\Delta}_1$ depends on whether force control or displacement control is utilized.

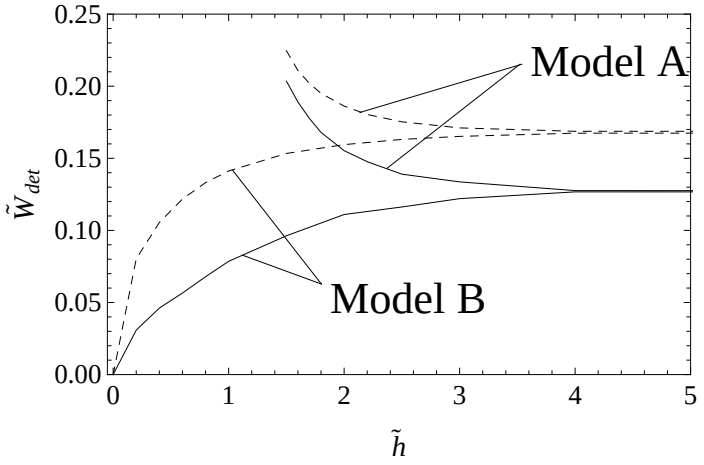

FIG. 9: The dimensionless energy dissipated during the pulling process as a function of the layer thickness. Calculations are performed under force controlled (solid lines) and displacement controlled (dashed lines) conditions. The displacement corresponding to the equilibrium state with positive contact area and no applied external load has been used as initial condition. Results are given for $\tilde{\Lambda} = 2$ and $\tilde{\gamma} = 0.05$.

Fig. 9 shows the dependence of $\tilde{W}_{\rm det}$ on the dimensionless layer thickness. Calculations are performed under force (solid lines) and displacement (dashed lines) controlled conditions. As expected, differences in behavior are found only for thin layers. In fact, for the model A, the work required for detachment strongly increases when the thickness is reduced, whereas, for model B, $\tilde{W}_{\rm det}$ decreases as thickness is decreased and asymptotically vanishes as $h \to 0$. This qualitative behavior is not affected by which condition (force control or displacement control) is enforced.

Notice the detachment work given in eq. (20) is valid for debonding from partial contact. Once the full contact is established, detachment may occur only if the pull-off pressure exceeds the theoretical adhesive van der Waals strength, which can be estimated as γ/ρ, where ρ is of the order of $1 - 10$ nm. However, under the JKR assumption, $\rho \to 0$, so there is no possibility to re-establish partial contact conditions, starting from complete contact. We notice that also considering real values of ρ, the resulting van der Waals stress would be so high (at least for the case of soft material) that a different debonding mechanism would occur before. This second mechanism (see, for example, Ref. [50]) involves the nucleation of small defects (or interfacial cracks) of nano- or micro-meter size which we do not investigate in our study.

B. Adhesiveless contact

In absence of adhesion, the contact between layer and substrate requires the mean pressure must be strictly positive.

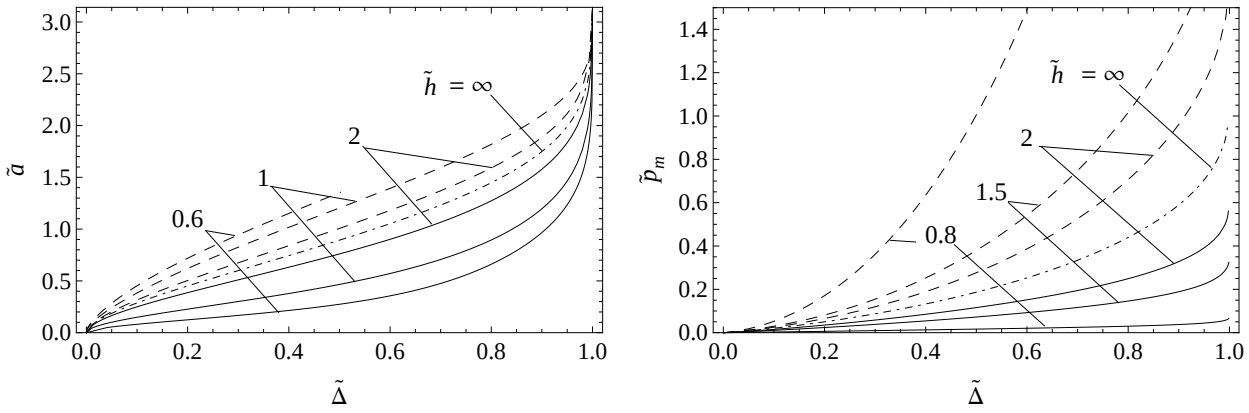

FIG. 10: The dimensionless contact size $\tilde{a}$ (a) and mean pressure $\tilde{p}_{\mathrm{m}}$ (b) at the equilibrium as functions of the dimensionless contact penetration $\tilde{\Delta}$, for different values of the dimensionless layer thickness $\tilde{h}$. Solid lines refers to the model A, dashed lines to the model B. The halfplane solution [51] is plotted with dashed-dot line.

Fig. 10 shows the dimensionless contact area (Fig. 10a) and mean pressure (Fig. 10b) as functions of the dimensionless contact penetration. As expected, the thickness of the layer significantly affects the contact behavior and strong differences are found depending on the upper boundary conditions of the layer. Moreover, in both cases, the Westergaard's solution [51] is recovered for layers of infinite thickness. As already observed, for the model B, the contact stiffness increases as the layer becomes thinner. This effect can be explained observing that, for relatively thin layers, the local deformation within the contact area can be estimated as $\varepsilon \approx \Delta/h$. As a result, at fixed displacement, the elastic energy stored at interface and the contact stiffness increase as the layer get thinner. The corresponding increase of the contact area (for thinner layers) is instead due to the interaction between the rigid confinement on the upper boundary and the material incompressibility ($\nu = 0.5$).

Viceversa, in the model A, the layer becomes more compliant and the contact area decreases by reducing the thickness. Such apparently counterintuitive behavior is explained observing that the overall stiffness of the layer is composed of two contributions (see Fig. 11): the first one is related to the layer bending stiffness $K_{\mathrm{flex}} \approx Eh^3/\lambda^3$, the latter is instead

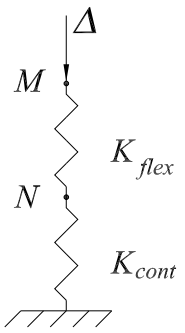

FIG. 11: The springs system equivalent to the model A in terms of overall stiffness.

related to the local stiffness of the layer near the contact K_{cont}, which can be estimated as $2Ea/h$. In fact, for not too large values of h, the interfacial elastic energy per unit length stored in the region close to the contact is $\mathcal{E} \approx (1/2)\, E\varepsilon^2 A$, where $\varepsilon \approx \Delta/h$ and $A \approx 2ah$ are, respectively, the local deformation and the size of the deformed region near the contact. Then, $\mathcal{E} \approx E\Delta^2\,(a/h)$ and the local stiffness per unit transversal width of the layer is $K_{\text{cont}} = \partial^2\mathcal{E}/\partial\Delta^2 \approx 2Ea/h$.

Therefore, for fixed penetration Δ (i.e. for fixed displacement of the point M in Fig. 11), the relative influence of the two contributions will depend on the layer thickness. In particular, when the layer is sufficiently thick, $K_{\text{flex}} >> K_{\text{cont}}$ and the displacement of the point N is $u\,(N) \approx \Delta$. In this case, the deformation is mainly located at the contact interface and we expect large contact areas. On the contrary, when the layer is thin, $K_{\text{flex}} << K_{\text{cont}}$ and $u\,(N) \approx 0$. As a result, the deformation is mainly governed by the bending stiffness of the layer and the contact area takes smaller values.

IV. CONCLUSIONS

In this paper, the adhesive and adhesiveless contact of an elastic slab on a slightly wavy rigid substrate is investigated. Two different constraint configurations are compared: a layer uniformly loaded on the upper free boundary (model A) and a layer rigidly confined on the upper boundary (model B).

In absence of adhesion, the model A shows a decreasing stiffness with reducing the layer thickness, whereas an opposite behavior is exhibited by the model B. In the limit of very thick layers, the classical Westergaard's solution of an elastic halfplane indented by a rigid sinusoidal profile is recovered in both cases.

In presence of adhesion, for the model A, partial contact can occur only if the layer thickness is larger than a threshold value h_{th}, which depends on the substrate amplitude. For the model B, instead, complete contact can occur only when the thickness is larger than the amplitude Λ of the rigid sinusoid. In the latter case, the layer jumps into full contact when the mean pressure reaches the peak value above which equilibrium in partial contact becomes unstable.

Moreover, the two models show different behaviors during the pulling process. As the thickness is reduced, the free layer exhibits a decreasing pull-off force and an increasing work of detachment, i.e. its adhesive toughness is enhanced by small thickness values. The confined layer, on the contrary, shows the opposite behavior: thinner layers entail larger adherence forces.

These results suggest the confined layer is more appropriate to characterize the behavior of structural adhesives or in general when the adhesive must resist to strong impulsive forces. The free layer, showing higher adhesive toughness, is suitable in all the applications where the strength of the adhesive joint depends on the amount of energy dissipated during the pulling process (soft adhesives, coatings and protective adhesives, pressure sensitive adhesives).

---

[1] Krahn, J., Liu, Y., Sadeghi, A., Menon, C. 2011 A tailless timing belt climbing platform utilizing dry adhesives with mushroom caps. Smart Mater. Struct. 20, 115021.

[2] Murphy, M.P., Kute, C., Menguc¸Y., Sitti, M. 2011 Waalbot II: adhesion recovery and improved performance of a climbing robot using fibrillar adhesives. Int. J. Robot. Res. 30, 118–133.

[3] Voigt, D., Karguth, A., Gorb, S. 2012 Shoe soles for the gripping robot: searching for polymer-based materials maximizing friction. Robot. Auton. Syst. 60, 1046–1055.

[4] Pugno, N. M. 2008 Spiderman gloves. Nanotoday 3, 35–41.

[5] Dillard, D. Advances in Structural Adhesive Bonding, Woodhead publishing limited, 2010.

[6] Sih G. C., Carpinteri A., Surace G., Advanced Technology for Design and Fabrication of Composite Materials and Structures: Applications to the Automotive, Marine, Aerospace and Construction Industry, Springer Science & Business Media, 2013.

[7] Kennar G. A., Interlayer for laminated safety glass, US Patent US4035549 A, 1977.

[8] Shaa, Y., Huib, C.Y., Kramerc, E.J., Garrettd P.D., Knapczyke J.W., Analysis of adhesion and interface debonding in laminated safety glass, Journal of Adhesion Science and Technology, 11 (1), 49-63, (1997).

[9] Piveteau L. -D., Girona M.I., Schlapbach L., Barboux P., Boilot J. -P., Gasser B., Thin films of calcium phosphate and titanium dioxide by a sol-gel route: a new method for coating medical implants, Journal of Materials Science: Materials in Medicine, 10(3), 161-167 (1999).

[10] Allen M., Myer B., Rushton, N., In Vitro and In Vivo Investigations into the Biocompatibility of Diamond-Like Carbon (DLC) Coatings for Orthopedic Applications, Journal of Biomedical Materials Research, 58(3), 319-328, (2001).

[11] Kwak, M. K., Jeong, H.-E., Suh, K. Y. 2011 Rational design and enhanced biocompatibility of a dry adhesive medical skin patch. Adv. Mater. 23, 3949–3953.

[12] Bacon, K.D., Cummins C.F., Pressure-sensitive adhesive, US Patent US2285570 A, 1942.

[13] Peterson D.R., Stupp, S.I., Poly(amino acid) adhesive tissue grafts, US Patent US5733868 A, 1998.

[14] Al-Harthi M. A., Bakather O. Y., De S.C., Pressure sensitive adhesive, US Patent US8697821 B1, 2014.

[15] Ding, J., Meng, Y., Wen, S.: Mechanical Stability and Sticking in a Model Microelectromechanical systems (MEMS) under Casimir Forces–Part II: The Role of the Casimir Effect. International Journal of Nonlinear Sciences and Numerical Simulation 1, 379–384 (2000)

[16] Ding, J., Wen, S., Meng, Y.: Theoretical study of the sticking of a membrane strip in MEMs under the Casimir effect. J Micromech Microeng 11, 202–208 (2001)

[17] Linder, C., Rooji, N.F.D.: Investigating on free-standing polysilicon beams in view of their applications as transducers. Sensors and Actuators A (Physical) 21(23), 1053–1059 (1990)

[18] Israelachvili, J.N., Tabor, D.: The measurement of van der Waals dispersion forces in the range 1.5 to 130 nm. Proc. R. Soc. A 331, 19–38 (1972)

[19] Tas, N., Sonnenberg, T., Jansen, H., Legtenberg, R., Elwenspoek, M.: Sticking in surface micromachining. J Micromech Microeng 6, 385–397 (1996).

[20] Carbone, G., Mangialardi, L. & Persson, B. N. J. 2004 Adhesion between a thin elastic plate, and a hard randomly rough substrate. Phys. Rev. B Cond. Matter Mater. Phys., 70, 125407.

[21] Hui, C.-Y., Glassmaker, N. J. & Jagota, A. 2005 How compliance compensates for surface roughness in fibrillar adhesion. J. Adhesion 81, 699–721.

[22] Persson, B. N. J. 2002 Adhesion between elastic bodies with randomly rough surfaces. Phys. Rev. Lett. 89, 245502.

[23] Guduru P.R., Detachment of a rigid solid from an elastic wavy surface: Theory, Journal of the Mechanics and Physics of Solids 55: 445-472, 2007.

[24] Guduru P.R. and Bull C., Detachment of a Rigid Solid from a Wavy Elastic Surface - Experiments, Journal of the Mechanics and Physics of Solids 55: 473-488, 2007.

[25] Carbone G., Mangialardi L., Analysis of adhesive contact of confined layers by using a Green's function approach, The Journal of the Mechanics and Physics of Solids, **56** (2), 684-706 (2008).

[26] Martina D., Creton C., Damman P., et al., Adhesion of soft viscoelastic adhesives on periodic rough surfaces, Soft Matter **8** (19), 5350-5357, doi: 10.1039/c2sm07059f (2012).

[27] Wu J-J., Numerical simulation of the adhesive contact between a slightly wavy surface and a half-space, Journal of Adhesion Science and Technology, 26, 331-351, 2012.

[28] G. Carbone, E. Pierro and G. Recchia, Loading-unloading hysteresis loop of randomly rough adhesive contacts, Physiscal Review E, in press.

[29] Gorb, S., Jiao, Y. & Scherge, M. 2000 Ultrastructural architecture and mechanical properties of attachment pads in Tettigonia viridissima (Orthoptera Tettigoniidae). J. Comp. Physiol. A 186, 821–831

[30] Gorb S., Varenberg M., Peressadko A.,Tuma J.,Biomimetic mushroom-shaped fibrillar adhesive microstructure. J. R. Soc. Interface 2007; 4: 271–5.

[31] Autumn, K., Liang, Y. A., Hsieh, S. T., Zesch, W., Chan, W. P., Kenny, T. W., Fearing, R. and Full, R. J. Adhesive force of a single gecko foot-hair, Nature, 405, 681–685 (2000).

[32] del Campo A. ,Greiner C. ,Artz E., Contact shape controls adhesion of bioinspired fibrillar surfaces. Langmuir 2007; 23: 10235–43.

[33] Dening K. ,Heepe L., Afferrante L.,Carbone G., Gorb S.N., Adhesion control by inflation: implications from biology to artificial attachment device. Appl. Phys. A 2014; 116: 567–73.

[34] Afferrante L., Carbone G., Demelio G., Pugno N.M., Adhesion of elastic thin films: double peeling of tapes versus axisymmetric peeling of membranes. Tribol. Lett. 2013; 52: 439–47.

[35] Glassmaker, N. J., Jagota, A., Hui, C.-Y., Noderer,W. L. & Chaudhury, M. K. 2007 Biologically inspired crack trapping for enhanced adhesion. Proc. Natl Acad. Sci. USA 104, 10 786–10 791.

[36] Afferrante L. and Carbone G., Biomimetic surfaces with controlled direction-dependent ad-

hesion, J. R. Soc. Interface 2012; 9: 3359-65.

[37] Afferrante L. and Carbone G., The mechanisms of detachment of mushroom-shaped micropillars: from defect propagation to membrane peeling. Macromol. React. Eng. 2013; 7: 609–15.

[38] Afferrante L., Grimaldi G., Demelio G. and Carbone G., 2015, Direction-dependent adhesion of micro-walls based biomimetic adhesives, International Journal of Adhesion & Adhesives, 61, 93–98.

[39] Hui, C.Y., Lin, Y.Y., aney, J.M. & Kramer, J.E., 2001, The Mechanics of Contact and Adhesion of Periodically Rough Surfaces, Journal of Polymer Science Part B: Polymer Physics, 39(11), 1195-1214.

[40] Martina, D., Creton C., Damman P., Jeusette M. & Lindner A. 2012 Adhesion of soft viscoelastic adhesives on periodic rough surfaces, Soft MAtter, 8, 5350.

[41] Dies, L., Restagno, F., Weil, R., Leger, L. & Poulard C., 2015, Role of adhesion between asperities in the formation of elastic solid/solid contacts, Eur. Phys. J. E, 38, 130.

[42] Ciavarella, M., Demelio, G., Barber, J. R., Jang, Y. H. Linear elastic contact of the Weierstrass profile. Proc. R. Soc. Lond. A, **456**, 387-405 (2000).

[43] Afferrante L. Ciavarella M. and Demelio G., Adhesive contact of the Weierstrass profile, Proc. R. Soc. A, 471: 20150248, 2015 (doi: 10.1098/rspa.2015.0248).

[44] Afferrante, L., Carbone, G., Demelio G. 2012 Interacting and coalescing Hertzian asperities: a new multiasperity contact model. Wear, **278–279,** 28–33.

[45] Landau, L.D., Lifshitz, E.M., 1959. Theory of Elasticity. Pergamon, London.

[46] Carbone G., Lorenz B., Persson B.N.J. and Wohlers A., Contact mechanics and rubber friction for randomly rough surfaces with anisotropic statistical properties, The European Physiscal Journal E – Soft Matter, **29** (3), 275–284, (2009).

[47] Carbone G., Mangialardi L., Adhesion and friction of an elastic half-space in contact with a slightly wavy rigid surface, Journal of the Mechanics and Physics of Solids, **52** (6), 1267-1287, 2004.

[48] Johnson, K.L. 1995 The adhesion of two elastic bodies with slightly wavy surfaces. Int. J. Solids Structures, **32** (No. 3/4), 423-430.

[49] Maugis, D., 2000. Contact Adhesion and Rupture of Elastic Solids. Springer, Berlin.

[50] Carbone, G., Pierro, E. & Gorb, N., Origin of the superior adhesive performance of mushroom-shaped microstructured surfaces. Soft Matter, **2011**, 7, 5545-5552.

[51] Westergaard, H.M., Bearing pressures and cracks.Trans.ASME, J.Appl.Mech.6, 49–53,1939.